

Temperature dependence of the optical properties of AlInN

L. F. Jiang,¹ W. Z. Shen,^{1,a)} and Q. X. Guo²

¹Department of Physics, Laboratory of Condensed Matter Spectroscopy and Opto-Electronic Physics, Shanghai Jiao Tong University, 1954 Hua Shan Road, Shanghai 200030, People's Republic of China

²Department of Electrical and Electronic Engineering, Synchrotron Light Application Center, Saga University, Saga 840-8502, Japan

(Received 7 March 2009; accepted 8 June 2009; published online 8 July 2009)

Measurements of the temperature dependence of transmission have been carried out on AlInN thin films grown by reactive radio-frequency magnetron sputtering on (0001) sapphire substrates. By following a detailed procedure developed for analyzing the transmission spectra, we obtained more reliable data for the effects of temperature on the optical properties of AlInN. Two sets of temperature and photon-energy dependence of empirical formulas have been established for the absorption coefficient, bandgap, Urbach bandtail, and refractive index, which not only unify various experimental data reported in the literature but also provide a database of the optical properties of AlInN based on experimental results. It was found that the shift in the temperature dependence of the bandgap increases with the Al content and that the Urbach bandtail parameter is closely related to the structural characteristics of the AlInN thin films. These optical properties provide an experimental basis for further theoretical investigation and the design of AlInN-based devices.

© 2009 American Institute of Physics. [DOI: 10.1063/1.3160299]

I. INTRODUCTION

With a wide variable bandgap range, ternary AlInN has great potential for applications in light-emitting diodes, laser diodes, solar cells, high-electron-mobility transistors, and highly reflective distributed Bragg reflectors in the ultraviolet (UV) region.^{1–5} For example, Al_{0.83}In_{0.17}N has been used as a strain free cladding layer on a GaN-based laser diode structure, leading to a reduction in the number of defects because it is lattice-matched to GaN.^{3–5} The material properties of AlInN alloys have been studied experimentally^{1–16} and theoretically.^{17–23} Starosta¹¹ synthesized AlInN polycrystalline films by a reactive multitarget sputtering method. Subsequently, the bandgap energy (E_g) of AlInN alloys has been obtained from the transmission spectra of such polycrystalline films, usually by linear extrapolation.^{12–16} However, without detailed theoretical analysis, E_g cannot be yielded accurately from the optical spectra owing to the poor absorption edge of AlInN.

It is possible to classify the absorption spectrum of AlInN into two regions: one is the intrinsic absorption region, which results from the optical transitions of electrons from the valence band to the conduction band, and the other is the Urbach absorption region, which results from interactions other than band-to-band transitions, such as electron holes, electron phonons, and electron impurities. Yamaguchi *et al.*^{14,15} reported both the intrinsic absorption coefficient (on the order of 10^4 – 10^5 cm⁻¹) and the Urbach bandtail energy (E_U) of Al_xIn_{1-x}N thin films grown by metalorganic vapor phase epitaxy with x from 0.42 to 0.86, but the tendency of E_U cannot be explained by the full width at half maximum (FWHM) of x-ray diffraction (XRD) spectra ob-

tained from their samples. Yeh *et al.*¹⁶ demonstrated a similar room-temperature intrinsic absorption coefficient for AlInN thin films grown by radio-frequency (RF) reactive sputtering. Furthermore, the refractive index (n) is another important parameter in the design of AlInN-based devices. Most researchers²⁴ have assumed n to be a constant value of 2.0 for AlInN with different Al contents, while Peng *et al.*¹³ demonstrated the photon-energy dependence of the room-temperature refractive index of Al_xIn_{1-x}N with x from 0.18 to 1.0 from the reflectivity spectra. To the best of our knowledge, there has been no systematic study of the temperature and wavelength dependences of the optical properties of AlInN thin films.

A detailed knowledge of the optical properties of AlInN thin films is both of scientific interest and of importance for device applications. In this paper, we present a comprehensive experimental and theoretical investigation of optical transmission, which not only provides much more reliable data for the optical properties of AlInN but also addresses the dependence of these optical properties on temperature, wavelength, and Al content. We further provide a database of the optical properties of AlInN based on experimental results by establishing two sets of temperature and photon-energy dependence of empirical formulas for the absorption coefficient, bandgap, Urbach bandtail, and refractive index.

II. EXPERIMENTAL DETAILS AND STRUCTURAL CHARACTERIZATION

The AlInN films were prepared on (0001) sapphire substrates by reactive RF magnetron sputtering in an ambient of argon and nitrogen.²⁵ The sapphire substrates were chemically cleaned, degreased in organic solvents, etched in an acid solution, and then rinsed in de-ionized water. During the growth, the substrate temperature, total gas flow rate, and pressure were maintained at 100 °C, 3 SCCM (SCCM de-

^{a)}Author to whom correspondence should be addressed. Electronic mail: wzshen@sjtu.edu.cn.

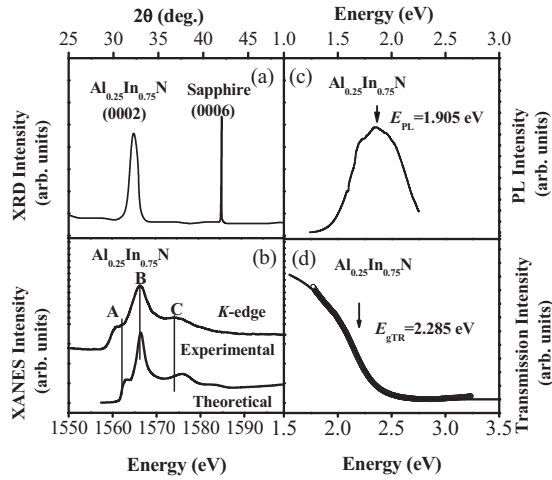


FIG. 1. (a) XRD, (b) Al *K*-edge XANES, (c) PL, and (d) transmission spectra of the $\text{Al}_{0.25}\text{In}_{0.75}\text{N}$ thin film at room temperature.

notes standard cubic centimeter per minute at STP), and 10 mTorr, respectively. Indium and aluminum plates were separately mounted onto the targets, and the sputtered area was varied to obtain AlInN films with the desired composition. The indium and aluminum plates were simultaneously sputtered at RF powers of 100 and 200 W, respectively, while the substrate was rotated at a constant rate of 30 rpm. Five AlInN samples with Al contents of 0, 0.05, 0.25, 0.40, and 1.0, and thicknesses of 0.690, 0.380, 0.315, 0.205, and 0.105 μm (obtained by a Tencor Instruments Alpha-step 200 device), respectively, were selected in the present study. The Al contents within the AlInN thin films were obtained by XRD measurements using a Philips X'Pert diffractometer and confirmed by x-ray absorption near-edge fine structure (XANES) experiments carried out at beam line BL1A of the UVSOR facility at the Institute for Molecular Science, Japan.² The temperature dependence of transmission was measured using a Jobin Yvon 460 monochromator. Photoluminescence (PL) spectra were recorded using a Jobin Yvon LabRAM HR 800UV micro-Raman system with an Andor DU420 classic charge-coupled-device detector.

Figure 1(a) shows the XRD pattern of the $\text{Al}_{0.25}\text{In}_{0.75}\text{N}$ thin film. The (0002) diffraction peak of AlInN can be observed together with the (0006) reflection from the sapphire substrate. Neither of the {102} and {103} peaks of AlInN, which have stronger intensity than the (0002) peak for a polycrystalline sample,¹³ were detected. This result suggests that the AlInN film is highly oriented in the *c*-plane with a wurtzite structure and that the *c*-axis of AlInN crystal is aligned normally to the substrate surface. The Al content was determined using Vegard's law, which states that the change in composition is proportional to the change in the lattice constant. Vegard's law is considered to be valid for determining the composition in III-V nitrides such as InGaN,^{26,27} and its validity for AlInN has been confirmed from the estimation of equilibrium volume by an *ab initio* pseudopotential calculation.¹⁷ Although the exact validity of Vegard's law in the case of AlInN has been challenged recently,²⁸ the reported deviations would not modify the derived InN mole fractions by more than 1% on an absolute scale.²⁹

Figure 1(b) shows the room-temperature experimental Al *K*-edge XANES spectra of the $\text{Al}_{0.25}\text{In}_{0.75}\text{N}$ thin film, as well as the theoretical results computed on the basis of self-consistent-field real-space multiple-scattering-theory calculations using the FEFF8 code,³⁰ showing three peaks A, B, and C. The main peak labeled B can be clearly observed in all samples that include Al. Its intensity increases with increasing Al content, although a linear relationship was not observed because the intensity depends on both the Al content and the sample thickness and size. By comparing the theoretical results with the experimental data, we find that the two spectra are in satisfactory agreement, although there are a few shifts in peak positions and differences in intensity, which may be due to errors in the theory.³⁰ We have demonstrated that the Al *K*-edge XANES spectra of AlInN films give indications of their composition.²

III. THEORETICAL MODEL

In modeling the transmission spectra of the AlInN thin film samples, we consider the multiple reflections at three interfaces: air to AlInN epilayer (thickness d_{AlInN}) (subscript 1), epilayer to transparent sapphire substrate (thickness d_{sapphire}) (subscript 2), and substrate to air (subscript 3). The transmission for light passing through the samples can then be calculated using

$$T_{1,3} = \frac{(1 - R_1)(1 - L)T_{2,3}a_1}{1 - R_1(1 - L)R_{2,3}a_1^2}, \quad (1)$$

with

$$T_{2,3} = \frac{(1 - R_2)(1 - R_3)a_2}{1 - R_2R_3a_2^2},$$

$$R_{2,3} = R_2 + \frac{R_3(1 - R_2)^2a_2^2}{1 - R_2R_3a_2^2},$$

$$a_1 = \exp(-\alpha_{\text{AlInN}}d_{\text{AlInN}}),$$

$$a_2 = \exp(-\alpha_{\text{sapphire}}d_{\text{sapphire}}).$$

The parameter L denotes the fraction of light loss at the epilayer surface and is treated as a variable to match the calculated transmission with the measured transmission. R_1 , R_2 , and R_3 are the reflectivities at the three interfaces, with corresponding subscripts, and can be obtained from

$$R = \frac{(n_i - n_j)^2}{(n_i + n_j)^2}. \quad (2)$$

The refractive indices of AlInN and sapphire can be obtained from the theoretical calculation using a modified dielectric function model proposed by Adachi.^{31,32} The real part ε_1 of the complex dielectric function $\varepsilon(E)$ as a function of energy E is described by the sum of four terms. They are the lowest direct gap E_0 dependence of the interband transition contribution ε_{1i} , the excitonic contribution ε_{1e} at the critical points E_0 , the free-carrier contribution ε_{1f} , and the

additive constant $\varepsilon_1(\infty)$, which is the background dielectric contribution arising from the higher-lying-gap transitions, such as the E_1 , $E_1 + \Delta_1$, and E_2 transitions.

The interband transition contribution ε_{1i} is obtained by a Lorentz calculation of the imaginary part of the dielectric function ε_{2i} for a collection of non interacting atoms.^{33,34} If a single transition is considered, ε_{2i} is given by

$$\varepsilon_{2i}(E) = \frac{AE_n CE}{(E^2 - E_n^2)^2 + C^2 E^2}, \quad E > E_g, \quad (3a)$$

$$\varepsilon_{2i}(E) = 0, \quad E \leq E_g, \quad (3b)$$

where A is the amplitude constant, E_n is the transition peak energy, C is the broadening term, and E_g is the bandgap. ε_{1i} can be obtained by Kramers–Kronig (KK) integration

$$\varepsilon_{1i}(E) = 1 + \frac{2}{\pi} P \int_{E_g}^{\infty} \frac{\xi \varepsilon_{2i}(\xi)}{\xi^2 - E^2} d\xi, \quad (4)$$

where P denotes the Cauchy principal part of the integral.

According to Ref. 35, the excitonic contribution ε_{1e} can be expressed as

$$\varepsilon_{1e}(E) = \sum_{m=1}^{\infty} \frac{A^{\text{ex}}_0}{m^3 [E_g - (G^{\text{3D}}_0/m^2) - E - i\Gamma_0]}, \quad (5)$$

where A^{ex}_0 is the three-dimensional (3D) exciton strength parameter, G^{3D}_0 is the 3D exciton binding energy, and Γ_0 is a damping broadening constant related to the lifetime broadening of the electronic states, which affects the dielectric function in the E_0 -gap region. Adachi^{31,32} showed that the model can explain the experimental dielectric function data accurately without taking into account the broadening constant. Therefore, we have also omitted Γ_0 in our model since no detailed information on Γ_0 for AlInN thin films is yet available. On the basis of the quasiclassical Boltzmann equation and Drude–Zener theory,³⁶ the free-carrier contribution ε_{1f} can be described as

$$\varepsilon_{1f}(E) = \varepsilon_{f\infty} - \omega_p^2 / \omega^2 = \varepsilon_{f\infty} - b/E^2, \quad (6)$$

where $\varepsilon_{f\infty}$ is the high-frequency dielectric constant of the lattice, $\omega_p^2 = (4\pi n_e e^2) / m^*$ is the plasma frequency, and e , n_e , and m^* are the electron charge, the free-electron concentration, and the effective electron mass, respectively.

By combining Eqs. (4) and (5) with Eq. (6), we obtain the following expression for ε_1 :

$$\varepsilon_1(E) = \varepsilon_{1\infty}(E) + \varepsilon_{1i}(E) + \varepsilon_{1e}(E) + \varepsilon_{f\infty}(E) - b/E^2, \quad (7)$$

where the contributions $\varepsilon_{1\infty}$ are due to the higher-lying bands (E_1 , $E_1 + \Delta_1$, and E_2). We can then obtain the imaginary part of the complex dielectric function using the KK transformation (KKT),³⁷

$$\varepsilon_2(E) = -\frac{2E}{\pi} \int_0^{\infty} \frac{\varepsilon_1(\xi)}{\xi^2 - E^2} d\xi. \quad (8)$$

Finally, the refractive index n can be obtained as follows:³⁸

$$n = \sqrt{\frac{(\varepsilon_1^2 + \varepsilon_2^2)^{1/2} + \varepsilon_1}{2}}. \quad (9)$$

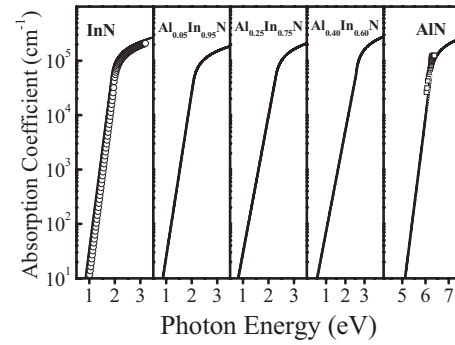


FIG. 2. Urbach and intrinsic absorption coefficient (solid curves) of the AlInN thin films at room temperature. The open circles and squares represent experimental data reported in Refs. 44 and 45, respectively.

Including the Urbach exponential absorption edge and the square root of intrinsic absorption, we can write the absorption coefficient of AlInN thin films as³⁹

$$\alpha(E) = \begin{cases} \alpha_0 \exp[(E - E_e)/E_U], & E < E_g \\ \alpha_d (E - E'_g)^{1/2}, & E \geq E_g \end{cases} \quad (10)$$

where the physical origins of the above four bandgap parameters are given as follows:^{39,40} E_e coincides roughly with the energy of the lowest free exciton energy at 0 K, E'_g is the bandgap energy of the material without bandtail distortions, and E_U is the Urbach bandtail parameter. These material parameters, including a_0 and a_d , are linked through their continuity at the energy bandgap E_g .

IV. RESULTS AND DISCUSSION

We start with the transmission and PL spectra of the AlInN thin films to obtain their detailed optical properties. Figures 1(c) and 1(d) show the room-temperature PL and transmission spectra (with the laser incidence normal to the surface and a peak energy E_{PL} of 1.905 eV) of the $\text{Al}_{0.25}\text{In}_{0.75}\text{N}$ film, respectively. It is clear that the theoretical transmission results calculated from Eqs. (1), (2), (3a), (3b), and (4)–(10) fit the experimental data very well, yielding a transmission energy E_{gTR} of 2.285 eV. From the PL and transmission spectra, an energy difference of about 380 meV is deduced, corresponding to a large Stokes shift compared with that usually measured in AlGaN or low-indium-content InGaN alloys.^{41,42} Such a large energy difference between the band edge and luminescence of AlInN has been observed by Butte *et al.*⁴³ and Wang *et al.*⁹ and can possibly be ascribed to fluctuations in the In composition or to the presence of deep defects or impurities acting as preferential recombination centers. Through the calculations for the temperature dependence of the transmission spectra, we can extract, as discussed below, the detailed temperature dependence of the optical properties of AlInN, such as the absorption coefficient α , bandgap E_g , Urbach bandtail parameter E_U , and refractive index n .

A. Absorption Coefficient

Figure 2 shows the obtained Urbach and intrinsic absorption coefficient (solid curves) of the AlInN thin films at room temperature. It can be clearly seen that the Urbach

TABLE I. Parameters for the set of empirical formulas [Eq. (11)] used to describe the temperature dependence of the absorption coefficient, bandgap, and Urbach bandtail in the AlInN thin films.

Samples	a_d (cm^{-1})		E_g (eV)		E_e (eV)		E'_g (eV)		E_U (meV)		β_8 (meV)		
	a_0 (10^4 cm^{-1})	a_2 (cm^{-1}/K)	$E_g(0)$ (eV)	β_1 ($10^{-4} \text{ eV}/\text{K}$)	β_2 (K)	$E_e(0)$ (eV)	β_3 ($10^{-4} \text{ eV}/\text{K}$)	β_4 (K)	$E'_g(0)$ (eV)	β_5 ($10^{-4} \text{ eV}/\text{K}$)		β_6 (K)	$E_U(0)$ (meV)
InN	3.5	32.2	1.881	4.00	570	1.865	3.81	470	1.840	4.01	570	90.8	4.35
Al _{0.05} In _{0.95} N	3.0	32.3	2.091	4.20	620	2.061	4.00	620	2.021	4.40	600	104.8	7.00
Al _{0.25} In _{0.75} N	4.0	69.6	2.350	9.11	1000	2.230	9.30	990	2.275	9.31	900	128.0	8.00
Al _{0.40} In _{0.60} N	4.5	30.4	2.610	10.70	1100	2.540	9.41	1500	2.253	9.41	1550	194.8	7.00
AlN	4.0	19.3	6.317	17.81	1400	6.296	17.60	1480	6.270	17.80	1400	69.1	5.54

exponential absorption and the square root of intrinsic absorption are closely linked at the turning points a_g (the absorption coefficient at $E=E_g$). To demonstrate the reliability of the obtained absorption coefficient, we have also shown in Fig. 2 the results reported in the literature for a direct comparison: the room-temperature absorption coefficients of InN from Ref. 44 (open circles) and AlN from Ref. 45 (open squares). It is clear that the present results are in reasonably good agreement with the data reported by our previous study and by the other group using a different growth method.

Furthermore, we established an overall empirical base for the temperature and photon-energy dependence of the absorption coefficient of AlInN through the absorption and bandgap parameters in Eq. (10). The absorption parameters a_0 and a_d are usually independent of temperature and proportional to temperature in semiconductors, respectively.⁴⁶ In the case of AlInN, the absorption parameter a_0 is also found to be a constant, while a_d has a linear dependence on temperature. The temperature dependence of the bandgap parameters E_g , E_e , and E'_g can be accurately described by the empirical Varshni equation. For the Urbach bandtail parameter E_U , we employed the theoretical dependence of the bandtail discussed in Sec. IV C. As a result, the overall absorption coefficient of AlInN can be described by Eq. (10) through the following empirical formulas:

$$\alpha_d = \alpha_1 - \alpha_2 T \quad (\text{cm}^{-1}),$$

$$\alpha_g = \alpha_0 \exp[(E_g - E_e)/E_U] \quad (\text{cm}^{-1}),$$

$$E_g(T) = E_g(0) - \beta_1 T^2 / (\beta_2 + T) \quad (\text{eV}),$$

$$E_e(T) = E_e(0) - \beta_3 T^2 / (\beta_4 + T) \quad (\text{eV}),$$

$$E'_g(T) = E'_g(0) - \beta_5 T^2 / (\beta_6 + T) \quad (\text{eV}),$$

$$E_U(T) = E_U(0) + \beta_7 T^{3/2} + \beta_8 \coth \frac{\hbar \omega_{\text{LO}}}{2k_B T} \quad (\text{meV}), \quad (11)$$

with the parameters in these formulas listed in Table I for different Al contents.

B. Energy Bandgap

The conventional method of linear extrapolation from transmission/absorption spectra is not very accurate for the determination of the energy bandgap, particularly for the case of a flat absorption edge. Our above detailed calculation of the transmission spectra yields a more reliable and precise bandgap E_g than that obtained from the conventional method of linear extrapolation. Figure 3(a) shows the obtained room-temperature transmission bandgap E_g (300 K) (closed circles) as a function of Al composition, together with the PL peak energy (open squares), as well as our very recently reported values for AlInN with different contents¹⁰ (open circles) and the experimental results for a high Al content reported by Kim *et al.*⁴⁷ (closed triangles). Wright and Nelson¹⁷ performed the first-principles calculations on the bandgap energy of AlInN using the plane-wave pseudopotential method, which is based on the Kohn–Sham formulation

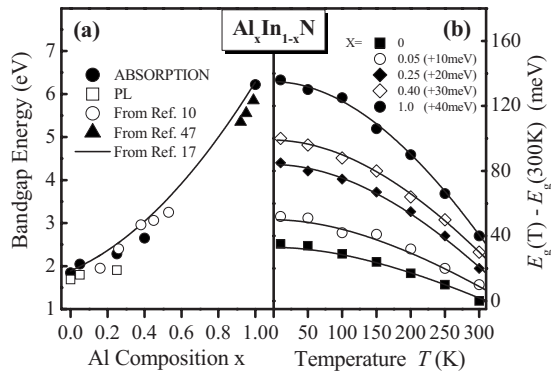


FIG. 3. (a) Room-temperature transmission bandgap E_g (300 K) (closed circles) as a function of Al composition, together with the PL peak energy (open squares), as well as our very recently reported values for AlInN with different contents from Ref. 10 (open circles) and the experimental results for a high Al content from Ref. 47 (closed triangles). The solid curve represents the values from Ref. 17 calculated by first principles. (b) Shift in the temperature dependence of the bandgap [$E_g(T) - E_g(300\text{ K})$] of the AlInN thin films, together with that obtained from the empirical Varshni fitting using Eq. (11) (solid curves with the fitting parameters listed in Table I).

of density-function theory. They argued that their results for the bowing parameter of wurtzite AlInN are correct because the predicted lattice constants and the c/a ratio are within about 1% of the measured experimental values. We have plotted their calculated values as a solid curve in Fig. 3(a). It was found that the listed experimental bandgap follows reasonably closely the theoretically predicted curve. Furthermore, we found that the difference between the transmission bandgap and PL peak energy, i.e., the Stokes shift, becomes large with increasing Al content ($x=0, 0.05, 0.25$), which has a similar tendency to the Urbach bandtail of the samples.

Figure 3(b) shows the shift in the temperature dependence of the bandgap [$E_g(T) - E_g(300\text{ K})$], together with that obtained from the empirical Varshni fitting of Eq. (11) (solid curves with the fitting parameters listed in Table I) of the AlInN thin films. The obtained parameters, β_1 (constant) of 0.40 meV/K and β_2 (Debye temperature) of 570 K, for InN are close to the tabulated values of 0.25 meV/K and 624 K.⁷ Moreover, it is interesting to note that the shift becomes large with increasing Al content. This is because the magnitude of the bandgap energy shift strongly depends on the V group elements in the III-V semiconductor compounds and increases in the order of N, Al, and As.⁴⁸ Equation (11) and Table I also give the temperature dependence of the other two bandgap parameters, E_e and E'_g , which have the same variation law as the energy bandgap E_g .

C. Urbach Bandtail

The temperature dependence of the bandtail characteristics in AlInN are also analyzed using our recently proposed bandtail theory,⁴⁹ which is based on the calculation of the density of occupied states and the carrier-phonon interaction using the adiabatic approximation. A quantitatively analytical formulation for the bandtail parameter E_U can be deduced by taking into account the structural disorder, carrier-impurity interaction (which mainly depends on carrier concentration

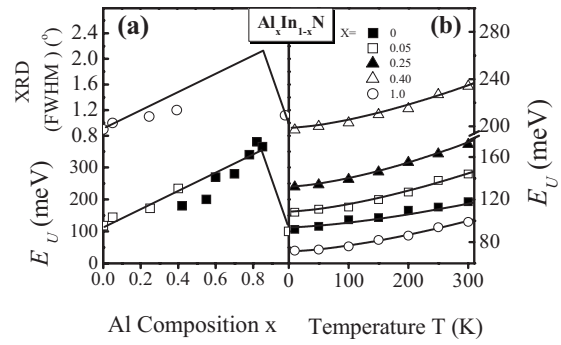


FIG. 4. (a) Room-temperature Urbach bandtail E_U (open squares) and FWHM obtained by XRD measurements of the AlInN thin films (open circles), together with bandtail data for other AlInN films from Ref. 15 (closed squares). (b) Temperature dependence of the Urbach bandtail E_U of the AlInN thin films, together with that obtained theoretically using Eq. (12) (solid curves with the fitting parameters listed in Table I).

and implicitly depends on temperature), and carrier-phonon interaction (which mainly depends on temperature), E_U has the form of⁴⁹

$$E_U(T) = \frac{1}{2}k_B U \theta_D + \frac{4\pi^2 Z^2 q^4 m^* L_D^3}{9\sqrt{3}\epsilon^2 \hbar^2} [(1 - 1/e)n_d + N_{BD}] + F \coth\left(\frac{\hbar\omega_{LO}}{2k_B T}\right), \quad (12)$$

where k_B is the Boltzmann constant, U is the lattice strain related to the structural disorder, θ_D is the Debye temperature, Z is the impurity charge, q is the electron charge, m^* is the carrier effective mass, ϵ is the static dielectric permittivity, \hbar is Planck's constant divided by 2π , n_d is the carrier concentration difference between the center n_0 and the surface of the grain (the grain boundary contribution), N_{BD} is the effective trap charge distribution (the grain defect contribution), F is a constant, and $\hbar\omega_{LO}$ [obtained by linear interpolation between the values of 995 cm^{-1} for AlN (Ref. 50) and 73 cm^{-1} for InN (Ref. 51)] is the longitudinal-optical (LO) phonon energy in AlInN (the thermal contribution). The Debye length L_D is given by

$$L_D = \left(\frac{\epsilon k_B T}{q^2 n_0}\right)^{1/2}. \quad (13)$$

The first term in the right-hand side of Eq. (12) is due to the contribution of structural disorder, which is independent of temperature, carrier concentration, and impurity concentration, and therefore can be regarded as constant for materials grown under the same growth conditions. The final equation of Eq. (11) is a simplified version of Eq. (12).

Figure 4(a) shows the room-temperature Urbach bandtail E_U for our AlInN films (open squares) together with bandtail data for other AlInN films from Ref. 15 (closed squares). It can be clearly seen that the bandtail E_U of AlInN increases linearly with Al content from 0 to 0.8, corresponding to the decrease in the structural quality observed by XRD with the FWHM shown as open circles, owing to the formation of lattice defects and disorder in the ternary structure. With a further increase in Al content, E_U is expected to decrease and approach the other binary AlN end. The same tendency of E_U

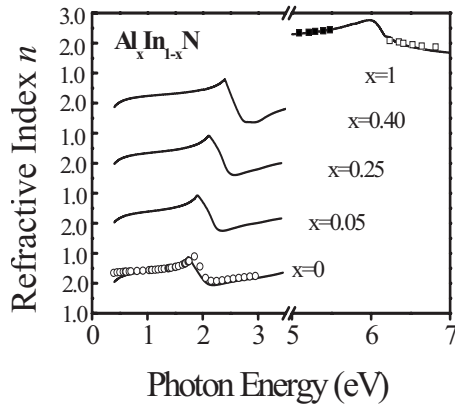


FIG. 5. Photon-energy dependence of the values of the refractive index n of AlInN with different Al contents at 300 K. Also shown for comparison are the refractive index reported in Ref. 52 (closed squares), Ref. 36 (open squares), and Ref. 44 (open circles).

has been found in the ternary AlGaIn system, whose maximum E_U is also at the Al content of 0.8.⁵² Figure 4(b) shows the obtained temperature dependence of the Urbach bandtail E_U of the AlInN films together with that obtained theoretically using Eq. (12) (solid curves with the fitting parameters listed in Table I). The good agreement demonstrates the reliability of the semiconductor bandtail theory.⁴⁹ In comparison with our previously reported temperature dependence of E_U for InN (Ref. 44) and AlN (Ref. 46) thin films, the obtained E_U for AlInN with different Al contents exhibits a similar temperature dependence. It was found that the structural disorder term dominates the interactive terms for the AlInN thin films. The thermal contribution of AlInN is only 2–4 meV at room temperature (300 K). The small thermal contribution due to the thermal displacement of the ions reveals that the carrier-phonon interaction in AlInN is weak.

D. Refractive Index

Finally, in Fig. 5 we show the photon-energy dependence of the refractive index n of AlInN with different Al contents at 300 K. A peak can be clearly observed in every refractive index spectrum. In the previous paper,⁴⁶ we explained the appearance of these peaks in semiconductors in detail using KKT analysis, the peak positions correspond approximately to the energy bandgaps. As a result, the peak position of the refractive index for AlInN shifts with changing Al content, exhibiting behavior closely related to that of the energy bandgap. At photon energies considerably above the bandgap, the refractive index increases with photon en-

ergy, which is due to higher-lying-gap transitions.⁴⁶ Furthermore, the reported data for n are also shown in Fig. 5 for a direct comparison: the closed squares represent data from Ref. 52, open squares represent data from Ref. 36, and open circles represent data from Ref. 44. There is good agreement between the reported data and our obtained values, further demonstrating the reliability of our results for AlInN.

To summarize the temperature and wavelength dependences of the refractive index characteristics of AlInN, we find that they can be described well by an empirical Sellmeier equation⁵³ through fitting the experimental data below the bandgap as follows:

$$n(\lambda, T)^2 = m_1 + m_2/[1 - (m_3/\lambda)^2] + m_4\lambda^2, \quad (14)$$

where m_1 , m_2 , m_3 , and m_4 are the fitting parameters, which depend on temperature T , and λ is the wavelength in μm . The best fit yields

$$m_1 = \gamma_1 - \eta_1 T,$$

$$m_2 = \gamma_2 - \eta_2 T,$$

$$m_3 = \gamma_3 - \eta_3 T,$$

$$m_4 = \gamma_4 - \eta_4 T, \quad (15)$$

with the parameters in these formulas listed in Table II for different Al contents.

Using the empirical formulas in Eqs. (14) and (15), we can obtain the refractive index as a function of temperature and wavelength for AlInN below the bandgap, as well as the rate of refractive index change with temperature dn/dT . Shown in Fig. 6 is the obtained temperature dependence of the refractive index of the five AlInN samples, together with the calculated results from the above Sellmeier equation (solid curves) at a photon energy of 1.7 eV (slightly above the obtained bandgap of InN). It can be seen that all the calculated results fit the data very well. In addition, we also found that the refractive index has a positive temperature coefficient, i.e., for InN it increases by 0.084 when the temperature increases from 10 to 300 K at 1.7 eV. The positive temperature coefficient, which can also be understood by considering the KKT,⁴⁶ is related to the negative temperature dependence of the AlInN energy bandgap shown in Fig. 3. The change in the refractive index with temperature decreases with increasing Al content in AlInN. The resultant values of dn/dT near the bandgap of $2.91 \times 10^{-4} \text{ K}^{-1}$ for

TABLE II. Parameters for the empirical Sellmeier equation [Eqs. (14) and (15)] used to describe the temperature dependence of the refractive index n of the AlInN films with different Al contents below the bandgap.

Samples	γ_1	η_1 ($10^{-4}/\text{K}$)	γ_2	η_2 ($10^{-4}/\text{K}$)	γ_3	η_3 ($10^{-5}/\text{K}$)	γ_4	η_4 ($10^{-6}/\text{K}$)
InN	5.091	1.492	0.623	2.018	0.618	5.027	-0.170	-9.912
Al _{0.05} In _{0.95} N	4.951	0.527	0.778	0.315	0.570	3.119	-0.170	-1.816
Al _{0.25} In _{0.75} N	4.757	0.134	0.792	0.143	0.511	5.562	-0.171	-5.878
Al _{0.40} In _{0.60} N	4.410	0.063	0.849	0.052	0.447	0.824	-0.172	-1.005
AlN	3.560	-7.065	0.458	7.011	0.197	0.642	-0.175	-1.913

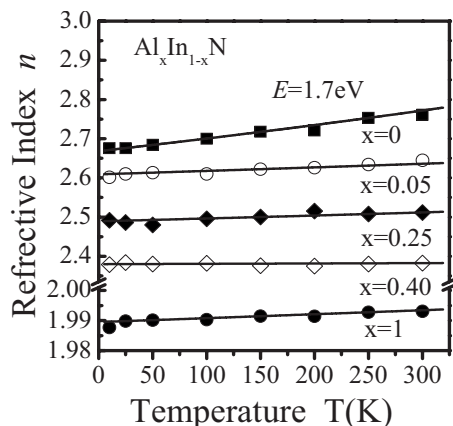


FIG. 6. Experimental temperature dependence of the refractive index of the AlInN thin films, together with the results calculated from the Sellmeier equation (solid curves), at a photon energy of 1.7 eV.

InN and $1.38 \times 10^{-4} \text{ K}^{-1}$ for AlN are close to our reported values of $3.04 \times 10^{-4} \text{ K}^{-1}$ in Ref. 44 and $1.56 \times 10^{-4} \text{ K}^{-1}$ in Ref. 46, respectively.

V. CONCLUSIONS

We have presented the results of a comprehensive experimental and theoretical study of AlInN thin films with different Al contents. By carrying out a detailed calculation of the transmission profile considering both the square root of intrinsic absorption and the Urbach exponential absorption edge, we demonstrated reasonably good agreement between the theoretical and experimental transmission. We determined the effects of temperature on the optical properties of AlInN, such as the absorption coefficient, bandgap, Urbach bandtail parameter, and refractive index. It was found that both the bandgap of AlInN and its shift with temperature become large with increasing Al contents and that the Urbach bandtail parameter is closely related to the structural characteristics. The temperature and photon-energy dependences of the absorption coefficient, bandgap, and Urbach bandtail parameter were described by a series of empirical formulas. The temperature dependence of the refractive index dispersion below the bandgap was found to obey a Sellmeier equation. These two sets of empirical formulas not only unify the various experimental data reported in the literature but also make a database of the optical properties of AlInN based on experimental results. All these optical properties are essential for the realization of AlInN-based devices.

ACKNOWLEDGMENTS

This work was supported by the Natural Science Foundation of China under Contract No. 10734020, Shanghai Municipal Key Project 08XD14022, the Graduate Innovation Foundation of Shanghai Jiao Tong University, and the Venture Business Laboratory of Saga University, Japan.

¹T. Seppanen, P. O. A. Persson, L. Hultman, J. Birch, and G. Z. Radnoczi, *J. Appl. Phys.* **97**, 083503 (2005).

²Q. X. Guo, J. Ding, T. Tanaka, M. Nishio, and H. Ogawa, *Appl. Phys. Lett.* **86**, 111911 (2005).

- ³J.-F. Carlin, J. Dorsaz, E. Feltin, R. Butte, N. Grandjean, M. Ilegems, and M. Laut, *Appl. Phys. Lett.* **86**, 031107 (2005).
- ⁴E. Feltin, J.-F. Carlin, J. Dorsaz, G. Christmann, R. Butte, M. Laut, M. Ilegems, and N. Grandjean, *Appl. Phys. Lett.* **88**, 051108 (2006).
- ⁵M. Gonschorek, J.-F. Carlin, E. Feltin, M. A. Py, and N. Grandjean, *Appl. Phys. Lett.* **89**, 062106 (2006).
- ⁶I. M. Watson, C. Liu, E. Gu, M. D. Dawson, P. R. Edwards, and R. W. Martin, *Appl. Phys. Lett.* **87**, 151901 (2005).
- ⁷K. Wang, R. W. Martin, E. Nogales, P. R. Edwards, K. P. O'Donnell, K. Lorenz, E. Alves, and I. M. Watson, *Appl. Phys. Lett.* **89**, 131912 (2006).
- ⁸A. Gadanez, J. Bläsing, A. Dadgar, C. Hums, and A. Krost, *Appl. Phys. Lett.* **90**, 221906 (2007).
- ⁹K. Wang, R. W. Martin, D. Amabile, P. R. Edwards, S. Hernandez, E. Nogales, K. P. O'Donnell, K. Lorenz, E. Alves, V. Matias, A. Vantomme, D. Wolferson, and I. M. Watson, *J. Appl. Phys.* **103**, 073510 (2008).
- ¹⁰Q. X. Guo, T. Tanaka, M. Nishio, and H. Ogawa, *Jpn. J. Appl. Phys.* **47**, 612 (2008).
- ¹¹K. Starosta, *Phys. Status Solidi A* **68**, K55 (1981).
- ¹²K. Kubota, Y. Kobayashi, and K. Fujimoto, *J. Appl. Phys.* **66**, 2984 (1989).
- ¹³T. Peng, J. Piprek, G. Qiu, J. O. Olowolafe, K. M. Unruh, C. P. Swann, and E. F. Schubert, *Appl. Phys. Lett.* **71**, 2439 (1997).
- ¹⁴S. Yamaguchi, M. Kariya, S. Nitta, T. Takeuchi, C. Wetzel, H. Amano, and I. Akasaki, *Appl. Phys. Lett.* **73**, 830 (1998).
- ¹⁵S. Yamaguchi, M. Kariya, S. Nitta, T. Takeuchi, C. Wetzel, H. Amano, and I. Akasaki, *Appl. Phys. Lett.* **76**, 876 (2000).
- ¹⁶T. S. Yeh, J. M. Wu, and W. H. Lan, *J. Cryst. Growth* **310**, 5308 (2008).
- ¹⁷A. F. Wright and J. S. Nelson, *Appl. Phys. Lett.* **66**, 3465 (1995).
- ¹⁸M. Goano, E. Bellotti, E. Ghillino, C. Garetto, G. Ghione, and K. F. Brennan, *J. Appl. Phys.* **88**, 6476 (2000).
- ¹⁹M. Ferhat and F. Bechstedt, *Phys. Rev. B* **65**, 075213 (2002).
- ²⁰Y. K. Kuo and W. W. Lin, *Jpn. J. Appl. Phys., Part 1* **41**, 5557 (2002).
- ²¹L. K. Teles, L. M. R. Scolfaro, J. Furthmüller, F. Bechstedt, and J. R. Leite, *J. Appl. Phys.* **92**, 7109 (2002).
- ²²B. T. Liou and C. W. Liu, *Opt. Commun.* **274**, 361 (2007).
- ²³V. Darakchieva, M. Y. Xie, F. Tasnadi, I. A. Abrikosov, L. Hultman, B. Monemar, J. Kamimura, and K. Kishino, *Appl. Phys. Lett.* **93**, 261908 (2008).
- ²⁴R. E. Jones, R. Broesler, K. M. Yu, J. W. Ager III, E. E. Haller, W. Walukiewicz, X. Chen, and W. J. Schaff, *J. Appl. Phys.* **104**, 123501 (2008).
- ²⁵Q. X. Guo, T. Tanaka, M. Nishio, and H. Ogawa, *Jpn. J. Appl. Phys., Part 2* **42**, L141 (2003).
- ²⁶Y. Koide, H. Itoh, N. Sawaki, I. Akasaki, and M. Hashimoto, *J. Electrochem. Soc.* **133**, 1956 (1986).
- ²⁷T. Nagatomo, T. Kuboyama, H. Minamino, and O. Omoto, *Jpn. J. Appl. Phys., Part 2* **28**, L1334 (1989).
- ²⁸K. Lorenz, N. Franco, E. Alves, I. M. Watson, R. W. Martin, and K. P. O'Donnell, *Phys. Rev. Lett.* **97**, 085501 (2006).
- ²⁹E. Iliopoulos, A. Adikimenakis, C. Giesen, M. Heuken, and A. Georgakilas, *Appl. Phys. Lett.* **92**, 191907 (2008).
- ³⁰A. L. Ankudinov, B. Travel, J. J. Rehr, and S. D. Conradson, *Phys. Rev. B* **58**, 7565 (1998).
- ³¹S. Adachi, *J. Appl. Phys.* **53**, 5863 (1982).
- ³²S. Adachi, *J. Appl. Phys.* **61**, 4869 (1987).
- ³³G. E. Jellison, Jr. and F. A. Modine, *Appl. Phys. Lett.* **69**, 371 (1996).
- ³⁴F. Wootton, *Optical Properties of Solids* (Academic, New York, 1972).
- ³⁵H. F. Yang, W. Z. Shen, Z. G. Qian, Q. J. Pang, H. Ogawa, and Q. X. Guo, *J. Appl. Phys.* **91**, 9803 (2002).
- ³⁶A. B. Djuricic and E. H. Li, *J. Appl. Phys.* **85**, 2848 (1999).
- ³⁷S. C. Shen, *Optical Properties of Semiconductors* (Academic, Beijing, 1992).
- ³⁸H. F. Yang, W. Z. Shen, and Q. J. Pang, *J. Phys.: Condens. Matter* **14**, 2067 (2002).
- ³⁹W. Z. Shen, *Int. J. Infrared Millim. Waves* **23**, 61 (2002).
- ⁴⁰C. F. Klingshirn, *Semiconductor Optics* (Springer-Verlag, Berlin, 1997).
- ⁴¹Y. H. Cho, G. H. Gainer, J. B. Lam, J. J. Song, W. Yang, and W. Jhe, *Phys. Rev. B* **61**, 7203 (2000).
- ⁴²C. Sasaki, H. Naito, M. Iwata, H. Kudo, Y. Yamada, T. Taguchi, T. Jyouchi, H. Okagawa, K. Tadatomo, and H. Tanaka, *J. Appl. Phys.* **93**, 1642 (2003).
- ⁴³R. Butte, J.-F. Carlin, E. Feltin, M. Gonschorek, S. Nicolay, G. Christmann, D. Simeonov, A. Castiglia, J. Dorsaz, H. J. Buehlmann, S.

- Christopoulos, G. B. H. von Hogerthal, A. J. D. Grundy, M. Mosca, C. Pinquier, M. A. Py, F. Demangeot, J. Frandon, P. G. Lagoudakis, J. J. Baumberg, and N. Grandjean, *J. Phys. D: Appl. Phys.* **40**, 6328 (2007).
- ⁴⁴L. F. Jiang, W. Z. Shen, H. F. Yang, H. Ogawa, and Q. X. Guo, *Appl. Phys. A: Mater. Sci. Process.* **78**, 89 (2004).
- ⁴⁵F. E. Fernandez, E. Rodriguez, M. Pumarol, T. Guzman, W. Jia, and A. Martinez, *Thin Solid Films* **377–378**, 781 (2000).
- ⁴⁶L. F. Jiang, W. Z. Shen, H. Ogawa, and Q. X. Guo, *J. Appl. Phys.* **94**, 5704 (2003).
- ⁴⁷K. S. Kim, A. Saxler, P. Kung, M. Razaghi, and K. Y. Lim, *Appl. Phys. Lett.* **71**, 800 (1997).
- ⁴⁸Q. X. Guo and A. Yoshida, *Jpn. J. Appl. Phys., Part 1* **33**, 2453 (1994).
- ⁴⁹W. Z. Shen, L. F. Jiang, H. F. Yang, F. Y. Meng, H. Ogawa, and Q. X. Guo, *Appl. Phys. Lett.* **80**, 2063 (2002).
- ⁵⁰C. T. M. Ribeiro, A. R. Zanatta, and F. Alvarez, *J. Non-Cryst. Solids* **299–302**, 323 (2002).
- ⁵¹T. Inushima, V. V. Mamutin, V. A. Vekshin, S. V. Ivanov, T. Sakon, M. Motokawa, and S. Ohoya, *J. Cryst. Growth* **227–228**, 481 (2001).
- ⁵²D. Brunner, H. Angerer, E. Bustarret, F. Freudenberg, R. Hopler, R. Dimitrov, O. Ambacher, and M. Stutzmann, *J. Appl. Phys.* **82**, 5090 (1997).
- ⁵³M. Born and E. Wolf, *Principles of Optics* (Pergamon, Oxford, 1984), Chap. 2.